Natural and Applied Sciences International Journal (NASIJ)
eISSN: 2788-4619 (online)
https://ideapublishers.org/index.php/nasij
Vol. 7, No. 1 (January-December), 2026, pp. 16-41
https://doi.org/10.47264/idea.nasij/7.1.2
Original Research Article

Multi-source geospatial analysis of the August 2025 cloudburst-induced flood in district Buner, Pakistan

Abdullah Khan*

Department of Space Science, Institute of Space Technology, Islamabad, Pakistan.

* Corresponding Author Email: abdullah11918114@gmail.com

Abstract:
This study analyzes the cloudburst-induced flood in Buner, Pakistan, in August 2025 through remote sensing and GIS-based multi-parametric criteria. The aim of this work is to define flood-prone areas by investigating the topography and validating the satellite-derived flood hazard areas for spatial modeling. Moreover, the CHIRPS daily precipitation, AW3D30 DEM, and Normalized Difference Water Index (NDWI) are studied from satellite images for the pre-and post-event. The rainfall analysis estimated the precipitation to be high, with a value of 66 mm/day on 15 August 2025, to induce a cloudburst event. The terrain survey revealed that the flood affected the low-elevation (357 to 900 m elevation) region with a slope of less than 6° to incur surface runoff. According to the weighted overlay model, three paramount parameters have been added (rainfall, 50%, slope 30%, and elevation 20%) in the Flood Hazard Index to subdivide the region of Buner into four zones of the hazard, i.e., Low, Moderate, High, and Very High. The results of testing the actual magnitude of the flood indicated that there was a good spatial compatibility of 88% of the flooding area, which was enclosed by the Very High Hazard area, thus providing evidence of the model. This study demonstrated the efficiency of the integration of remote sensing indices, rainfall data, and topographic parameters into a GIS environment to perform a rapid evaluation of the risks of floods.

Article History

Received:
10-Jan-2026

Revised:
25-Apr-2026

Re-revised:
02-Jul-2026

Accepted:
04-Jul-2026

Published:
17-Jul-2026

Keywords: Normalized difference index, Flood hazard index, Cloudburst, Flood, Remote sensing, GIS, Flood prone area, Flood hazard areas, Spatial modelling.

How to Cite:
Khan, A. (2026). Multi-source geospatial analysis of the August 2025 cloudburst-induced flood in district Buner, Pakistan. *Natural and Applied Sciences International Journal (NASIJ), 7*(1), 16-41. https://doi.org/10.47264/idea.nasij/7.1.2

1. Introduction

One of the most devastating natural risks that happens around the world annually is floods that cause massive socio-economic losses, damage to the environment, and even loss of human lives (Smith & Ward, 2020; Alfieri et al., 2017). In South Asia, the rapid topography monsoon system and growing settlements considerably increase the occurrence and severity of floods especially flash flooding caused by the extreme amount of rainfall like cloudbursts (Karki et al., 2017; Shrestha et al., 2020). Hydrometeorological extremes that cause flash flooding due to cloudbursts are also quite prevalent and increase in the mountainous regions due to climate change (Khan et al., 2022; IPCC, 2022). The recent research insists on the fact that flash flooding generated by cloudbursts is fast gives little time to evacuate and in the majority of cases affects communities who live in areas adjacent to river channels valley bottoms and low lying basins (Dimri et al., 2015; Bhatt et al., 2022).

Flood dynamics mapping inundation extent and hazard susceptibility have become rather important to understand with the help of remote sensing and Geographic Information Systems (GIS) (Schumann et al., 2018; Brivio et al., 2002). The optical indices of the satellite like the Normalized Difference Water Index (NDWI) are valid in the sense that an inundation change can be detected when pre and post event images are accessible to identify the change (McFeeters, 1996; Du et al., 2016). Nevertheless, cloud cover also restricts optical data in severe rains which is one of the significant limitations in cloudburst cases (Zhou et al., 2021). Although it is not an easy task Sentinel-2 multispectral imagery is quite common due to its spatial resolution (10 m) and a relatively short revisit period which make it an adequate instrument when it comes to identifying an event flood (Benoudjit et al., 2020; Mandal et al., 2023).

Digital Elevation Models (DEMs) including AW3D30, SRTM, and ASTER are popular topographic analysis tools because the terrain parameters including elevation and slope have a strong influence on the velocity of runoff accumulation areas and routes of floods (Kamp et al., 2021; Pham et al., 2021). Research has also indicated that the valleys with low altitude and low slopes are prone to floods whereas steep slopes allow rapid drainage (Rahman et al., 2023; Das et al., 2020). However, there are limitations to the DEM based analyses such as vertical errors mismatch or potential artefacts in mountainous areas (Gesch et al., 2018; O'Loughlin et al., 2020).

Rainfall data derived by satellites including Climate Hazards Group Infrared Precipitation with Station Data (CHIRPS) have been widely utilized to track extreme precipitation and prove hydrological processes (Funk et al., 2015; Tote et al., 2015). CHIRPS also provides long term rather global estimates of rainfall at relatively small spatial resolution the data is likely to be inaccurate in capturing localized cloudbursts in mountainous areas as it is spatially smoothed (Dinku et al., 2018; Kimani et al., 2017). Nevertheless, CHIRPS is among the best datasets to use in studying trends in precipitation in data deficient areas of Pakistan and the Himalayan belt (Ashouri et al., 2016).

Multi criteria GIS overlay based models of Flood Hazard Index (FHI) have been adopted as popular in mapping the susceptibility of flooding. The models would typically combine the terrain aspects, the intensity of rainfall, land cover, drainage patterns, and hydrologic indices to calculate the composite hazard surfaces (Tehrany et al., 2014; Samanta et al., 2018). The benefits of weighted overlay and AHP-based models are that it is possible to consider the experience of specialists and weight the parameter by regions (Saaty, 1980; Ahmad et al., 2020). Nevertheless, they are prone to the choice of weights, and unbiased outcomes may be demonstrated in case validation is not carried out with actual flood data (Kazakis et al., 2015; Khosrowavi et al., 2016). Thus, to assess the level of model reliability and minimize uncertainty it is necessary to combine the results of satellite derived flood extent with FHI data (Rahmati et al., 2016; Meraj et al., 2022).

The flash floods caused by cloudbursts have been on the rise in Pakistan mountainous districts because of the altered climatic regimes, anthropogenic stress, and unplanned settlement expansion (Shamshad et al., 2021; Farooq et al., 2019). Although much has been done in satellite based monitoring of floods there still exist glaring gaps in near-real-time evaluation, high resolution terrain precipitation interaction evaluation, and validated hazard algorithms of cloudburst prone catchments. To ensure that these gaps are addressed multi source geospatial data should be incorporated to improve on the spatial dynamics of the extreme rainfall induced flooding.

The objective of the current research is to come up with a complete remote sensing driven flood evaluation framework of cloudburst driven flash flood event that came to hit Buner District in August 2025. The main goal of the study is to combine and use multi source geospatial data sets with Sentinel-2 based NDWI, CHIRPS precipitation, AW3D30 terrain parameters such as both the surface and subsurface parameters to establish an accurate flood extent to examine the effects of the topography on the control factors and to model the vulnerability to flood. In particular, the research traces spatial distribution of floodwater on the basis of pre and post event NDWI. It analyses terrain effects in terms of elevation, slope, and hillshade. It also develops a Flood Hazard Index (FHI) based on a weighted overlay of rainfall, slope, and elevation. And it confirms the hazard model by measuring the spatial correlation between the forecasted hazard areas and the real inundation. This research offers a powerful decision support tool to intelligible the dynamics of floods in steep geomorphologically difficult areas like Buner as well as represents a repeatable methodology to future flood risk evaluation in cloud bursting prone areas of northern Pakistan by integrating hydrometeorological data terrain parameters with satellite generated flood mapping.

1.1. Study area

The study focuses on Buner district located of Khyber Pakhtunkhwa (KPK) province of Pakistan, which experienced a severe cloudburst-induced flash flood between 13 and 15 August 2025. The geographical location of this district is between 34.3943° N, 72.6151° E, encompassing an area of approximately 1,865 km² (Government of Khyber Pakhtunkhwa, 2023). It is bounded by Swat district to the north, Malakand to the west, Mardan to the south, and Shangla to the east. The topography of Buner is highly variable, consisting of rugged mountains, deeply incised valleys, and low lying alluvial plains (SMEDA, 2020). The elevations range from 357 m in the southern plains to over 3,037 m in the northern highlands, as derived from the AW3D30m. The elevation map showing high mountainous regions in red to yellow and low-elevation flood prone zones in blue to better visualize terrain morphology (Figure 1a). Similarly, a 3D hillshade model was generated using the same DEM (Figure 1b). The hillshade is used to identify the relief and geomorphological form of the district to underline steep ridges, valley bottoms, and foothill areas. These features play a critical role in directing flood flow paths and identifying areas vulnerable to surface runoff accumulation. The climate of Buner lies in a humid subtropical to semi-arid zone and it is receiving most of its rainfall during the monsoon season (July–September). Annual precipitation varies between 700 and 1200 mm, primarily influenced by the southwest monsoon system (Pakistan Meteorological Department, 2022). However, the combination of steep topography, sparse vegetation cover, and unplanned human settlements enhances the district's susceptibility to flash floods and landslides (Ali et al., 2019).

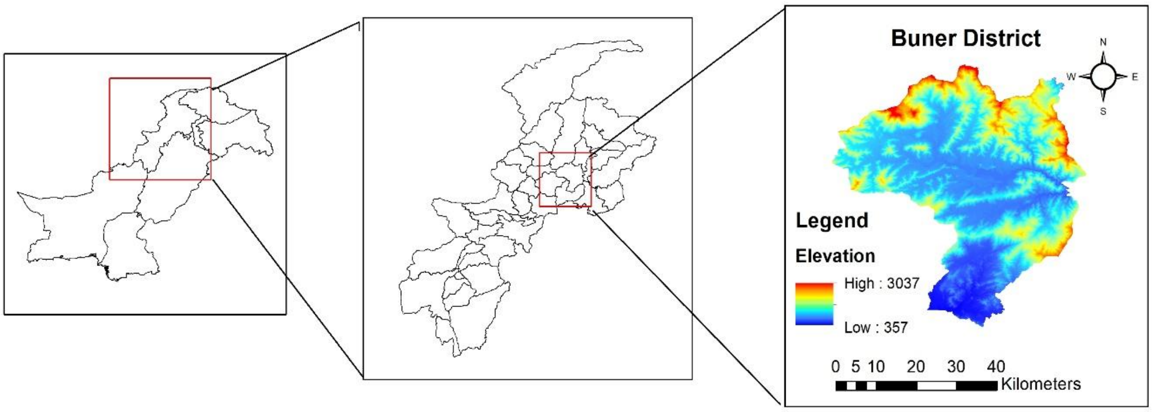

Figure 1a: The elevation map of Buner district derived from AW3D30 DEM (357–3037 m).

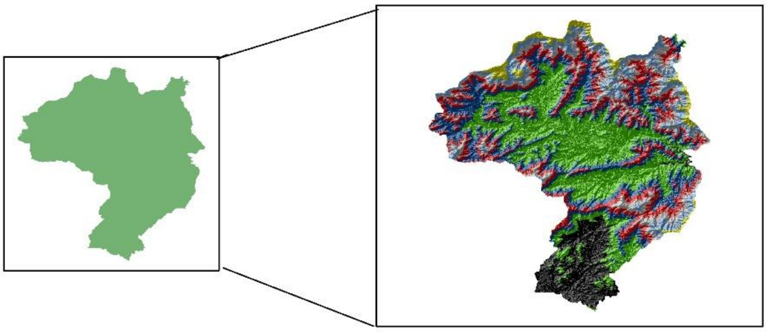

Figure 1b: The 3D hillshade visualization of Buner district showing terrain morphology and drainage valleys.

2. Methodology

2.1. Data collection and preparation

For this study, data from different satellites are processed in GIS to form an integrated version of flash flood measurement (Table 1).

Table 1. Data and their sources with the purpose mentioned.

Dataset	Source/Resolution	Purpose
AW3D30 DEM (30 m)	JAXA(30 meter)	Terrain analysis (elevation, slope, aspect, hillshade)
Sentinel-2 imagery	ESA(10 meter)	Pre- and post-flood NDWI flood detection
CHIRPS rainfall data	UCSB CHC (5 kilometers)	Rainfall intensity and cloudburst detection
Administrative boundary	Survey of Pakistan	AOI clipping and extraction
PDMA / field data	PDMA KPK reports	Damage and casualty validation

All datasets were clipped to Buner District and reprojected to WGS 1984 UTM Zone 43N for consistency in spatial analysis.

2.2. Terrain and hydrological analysis

Terrain and hydrological characteristics play a fundamental role in determining flood behavior, water accumulation, and flow dynamics, especially in mountainous catchments such as Buner district**.** To evaluate the influence of topography in the August 2025 cloudburst-induced flood, DEM data from the AW3D30m (A stands for ALOS (Advanced Land Observing Satellite), W stands for World, 3D is a 3-Dimensional map or model which means the elevation data (Digital Surface Model/Digital Elevation Model), and the 30m represents the horizontal resolution of the data which is about 30meters mesh (1 arc second separation)) dataset were used to derive elevation, slope, and hillshade layers within the ArcGIS 10.8 environment.

The AW3D30 dataset developed by the Japan Aerospace Exploration Agency (JAXA), offers a 30m spatial resolution to further make it suitable for local scale hydrological and geomorphological studies in rugged terrain (Takaku et al., 2020). The DEM was first preprocessed by clipping it to the Buner District boundary to ensure spatial consistency with other datasets. Three key topographic parameters elevation, slope, and hillshade were generated using the Spatial Analyst Tools in ArcMap.

2.2.1. Elevation classification

The DEM derived from the AW3D30 dataset was classified into seven elevation bands to represent the topographic variation across Buner District. The classified ranges included 357 to 600 m, 600 to 900 m, 900 to 1200 m, 1200 to 1500 m, 1500 to 1800 m, 1800 to 2500 m, and 2500 to 3037 m. These intervals were determined based on natural terrain breaks and the hydrological characteristics of the area. Analysis revealed that the low elevation zones between 357 and 900 m encompass the major flood prone valleys where runoff from the 13 to 15 August 2025 cloudburst event accumulated most intensively.

Overlaying the NDWI derived flood extent on the elevation map confirmed that the majority of inundation occurred within these lower bands. In contrast, areas above 1500 m showed minimal flood impact due to steep gradients and limited surface water retention capacity. The elevation analysis emphasizes the critical role of topography in flood dynamics, where low lying basins act as natural catchments for cloudburst induced runoff. This relationship aligns with previous findings that low altitude zones in mountain foothills are highly vulnerable to flash floods (Rahmati et al., 2019; Khosravi et al., 2016).

2.2.2. Slope classification

The slope raster was generated from AW3D30m DEM Using the Slope tool in ArcGIS to evaluate the influence of terrain gradient on flood distribution. The slope values were classified into five terrain categories: 0 to 2° (flat), 2° to 6° (gentle), 6° to 15° (moderate), 15° to 35° (steep) and >35° (very steep). This classification reflects the varying potential for water retention and surface runoff across the district. Result revealed that the major flood affected zones were concentrated within the flat (0 to 2°) and gentle slope (2° to 6°) categories which collectively cover a significant portion of the valley floors. The mean slope value of 4.17 across the flooded region further confirms that inundation primarily occurred in low gradient areas where reduced surface runoff facilitated water accumulation and longer flood residence times. The Areas with slopes greater than 15 mostly located in the northern and northeastern mountainous zones showed minimal flood impact due to their high runoff potential and rapid drainage. These findings align with previous research indicating that gentle slopes enhance water pooling while steep slopes accelerate runoff and limit floodwater retention (Rahman et al., 2023; Youssef et al., 2016)

2.2.3. Hillshade generation

A hillshade layer was generated from the DEM using azimuth 315° and altitude 45° simulating sunlight from the northwest to enhance terrain visualization. This step improved the interpretation of geomorphological features such as ridges, valleys, and drainage pathways (Singh et al., 2024). The hillshade model revealed that inundation primarily followed valley bottoms and depressions, where slope gradients and elevation were both minimal. Darker tones represented high relief zones while lighter areas corresponded to flatter plains that were more prone to flood accumulation.

2.2.4. Zonal statistics and flood relationship

The “Zonal Statistics as Table” tool was used to compute terrain metrics within the flood extent polygons derived from the post flood NDWI map. Results indicated a mean elevation of 799 m and a mean slope of 4.17° in flooded areas. These values confirm that flooding was concentrated in low-lying gently sloped zones consistent with the expected hydrodynamic behavior during high-intensity cloudburst events.

2.3. Rainfall and cloudburst analysis

Rainfall is the primary triggering factor in flash flood generation particularly in mountainous regions where short duration high intensity precipitation leads to rapid surface runoff and inundation. In this study, CHIRPS (Climate Hazards Group Infrared Precipitation with Station data) was employed to analyze rainfall distribution across Buner District for the period 10 to 17 August 2025**.** CHIRPS offers a quasi-global precipitation record at a spatial resolution of 0.05° (~5 km) merging satellite based infrared estimates with in-situ station data to generate reliable rainfall information for data scarce regions (Funk et al., 2015). Temporal analysis revealed a notable rainfall peak of 66.12 mm on 15 August 2025 confirming the occurrence of a cloudburst event that triggered extensive flooding across the district. The daily rainfall time series clearly indicates a sudden surge in precipitation intensity between 14 to 15 August which is characteristic of localized convective storms in hilly terrain (Sharma et al., 2023).

2.4. Topographic influence on flood distribution

2.4.1. Slope distribution of flooded pixels

The flood extent raster based on NDWI was overlaid on the slope raster to determine the distribution of floods in various slope categories through the use of a raster overlay method (Combine tool). The process allowed determining the presence of pixels that were flooded in each slope class. The resulting attribute table was then used to get the number of pixels that represented flooded areas in each slope category. The counts were then translated into the percentages to determine the relative occurrence of flooding by slope classes.

2.4.2. Elevation distribution of flooded

The raster overlay method (Combine tool) was used to overlay the raster of flooding with the elevation raster of various levels in order to analyze the distribution of floods in various elevation zones. This operation made it possible to detect the number of pixels that were flooded in each elevation band. The resulting attribute table was utilized to distill the number of pixels that were a result of flooding in each elevation category. The counts were then transformed into percentage values to measure relative frequencies of the flooding in the different elevation ranges.

2.5. Flood extent mapping using NDWI

Flood inundation mapping was performed using Sentinel-2 multispectral imagery to delineate areas affected by the August 2025 cloudburst event in Buner District. Two image were selected to represent the pre flood (20 July to 13 August 2025) and post flood (15 to 28 August 2025) periods. The NDWI was applied to both datasets to enhance open-water features and differentiate them from vegetation and soil surfaces. NDWI was computed using the equation:

$$\text{NDWI} = \frac{(Green - Near\ Infrared)}{(Green + Near\ Infrared)} \quad (1)$$

Where the Green band corresponds to Band 3 (0.56 μm**)** and the Near-Infrared (NIR) band corresponds to Band 8 (0.84 μm) of Sentinel-2 (McFeeters, 1996). Pixels with NDWI values greater than 0.3 were classified as water bodies, while those below the threshold were considered non-water surfaces. The threshold was selected based on visual inspection and prior studies demonstrating its reliability for flood detection (Xu, 2006; Acharya et al., 2018). The difference between the pre- and post-flood NDWI layers was computed to isolate newly inundated areas, which represented the flood extent resulting from the 13-15 August 2025 cloudburst.

The resulting flood extent raster was vectorized to produce a polygon shape file of the affected zones. This layer was later used in spatial overlay with elevation, slope, and rainfall datasets to evaluate flood vulnerability and topographic context. The NDWI based approach effectively delineates water surfaces even in complex topographic and vegetated regions providing a rapid and accurate method for post disaster assessment using freely available optical data from the Sentinel-2 MSI sensor (10 m resolution) (Li et al., 2020).

2.6. Flood Hazard Index (FHI) mapping

The FHI model was created based on a weighted overlay method that combined rainfall, slope and elevation. Each layer was re-categorized under five levels of hazards (1 to 5) and weight was given according to their influence. 0.50 Rainfall, 0.30 Slope, and 0.20 Elevation we can see in the Equation 2.

FHI= 0.5 x Rainfall (Raster image) +0.3 x Slope (Raster image) +0.2 x Elevation (Raster image) (2)

This FHI raster was also reclassified into four hazard classes namely Low, Moderate, high and very high.

2.7. Validation

The flood extent obtained with the use of the NDWI was superimposed onto a FHI map. The Zonal Statistics, as Table, was computed to determine the predictive power of the FHI model by computing the area of each hazard class that was flooded.

3. Results and discussion

3.1. DEM and flood extent

The topographical effect on the occurrence of floods was studied based on the AW3D30m data (30 m) to obtain the DEM. The minimum and maximum heights are 357 m in the southern plains and 3037 m in the mountainous areas in the north respectively. The difference depicts a rugged terrain whereby the direction and extent of runoff are directly proportional to elevation whereby overlaying the 2025 extent of flood on the DEM (Figure 2) the low lying areas below 900 m were predominantly inundated. The areas are associated with river basins and flat terrains where drainage converges thus making the areas highly prone to floods. On the other hand, uplands that were located above 1500 m did not experience much or no floods because of the steep slopes and rapid runoffs. Therefore the elevation flood correlation shows that topography is the overriding parameter that determines the concentration of floods in Buner. The findings validate that the 2025 flood caused by cloudbursts adhered to the depressures of the natural valley and settled in the shallow basins.

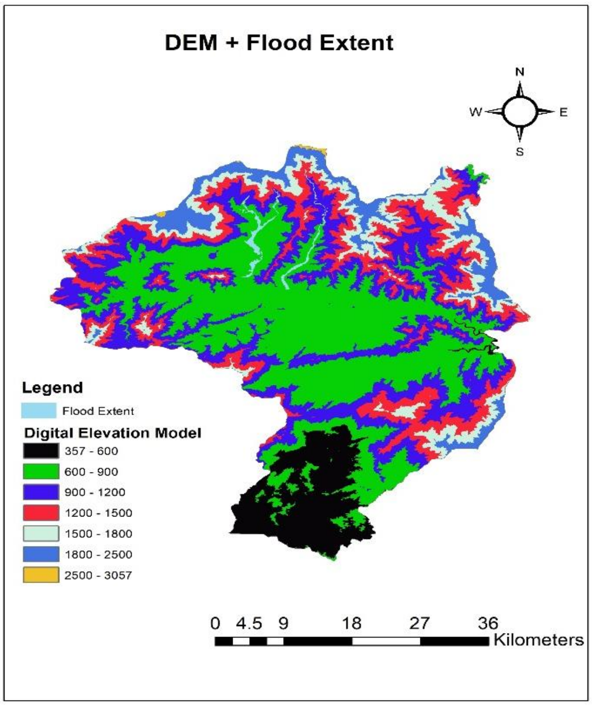

Figure 2: DEM and Flood Extent Map of Buner District (Elevation Range: 357–3037 m)

3.2 Slope Analysis

The slope layer which was based on the DEM was categorized into five to interpret the terrain steepness Table (2). 0 to 2° (Flat), 2° to 6° (Gentle), 6° to 15° (Moderate), 15° to 35° (Steep), and greater than 35° (Very Steep). As seen in the slope map (Figure 3) most of the flood infested regions fall in the 0 to 6° terrain which depict flat to gently inclined features. These circumstances contribute to water stagnation and surface stalling, particularly at central Buner around Dagar, Pir Baba, Bagra, Bhai Kaly, Ghazi Khan Kaly, Arshad Nagar, Bishnoye Kaly, and Pacha Kaly and the effects of the 2025 flood were worst. The slopes are steeper (greater than 15°) in the north of Buner which allows the runoff to happen very fast reducing the retention of floods and consequently reduces the chance of hazard.

The spatial association between slope and flood area indicates that the flattened and low topography area is closely associated with the flood area, as noted by NDWI. This observation is further supported by the statistical analysis with a mean slope of 4.17° in flooded areas, meaning that the general relief of the zone is gentle, allowing water pooling. The statistical summary of slope values (Table 3) indicates that the flood-affected area has a mean slope of 4.17°, suggesting predominantly gentle terrain favorable for water accumulation. The minimum slope (0°**)** confirms the presence of flat valley bottoms, while the maximum slope (50.19°) represents steep mountainous areas contributing to runoff. The moderate standard deviation (5.83°) reflects the variable topography but an overall dominance of low gradient terrain, which aligns with the spatial pattern of the 2025 flood extent observed on the slope map (Figure 3).

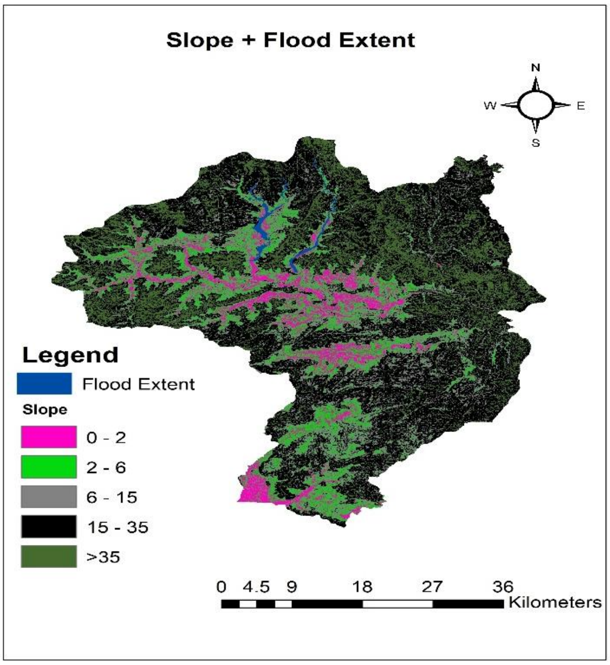

Figure 3: Slope Classification Map of Buner District

Table 2. Slope Classification of Buner District Derived from AW3D30 DEM

Class No	Slope Range (°)	Terrain Category	Flood Susceptibility
1	0 – 2°	Flat	Very High
2	2°– 6°	Gentle	High
3	6° – 15°	Moderate	Moderate
4	15°– 35°	Steep	Low
5	> 35°	Very Steep	Very Low

Table 3: Summary of Slope Statistics in Flooded Zones (Mean Slope = 4.17°)

Statistic	Value	Description
Count	11,369	Total raster cells (pixels) within the flooded zone used in slope analysis
Area (km²)	0.001009	Total analyzed area represented by one raster cell (per pixel basis)
Minimum Slope (°)	0.00	Lowest slope value indicating flat terrain
Maximum Slope (°)	50.19	Steepest slope within the analysis area
Range (°)	50.19	Difference between maximum and minimum slope
Mean Slope (°)	4.17°	Average slope value showing overall gentle terrain in flooded zones
Standard Deviation (°)	5.83	Variability of slope moderate terrain undulation
Sum	57,943.39	Total cumulative slope of all analyzed pixels

3.3. Hill shade analysis

The hillshade model (Figure 4) gave a realistic three dimensional view of the terrain where drainage pattern ridges and valleys could be seen in the Buner District. The hillshade was created with light source of 315° azimuths and 45° elevations which was an imitation of the sun at the northwest. The raster values would be between 0 up to 180 with 0 to 60 being greenish areas which are steep and elevated and 60 to 120 being moderately lit areas which are flat topped surfaces and which would collect floodwater. The overlay of the flood extent of 2025 and the hillshade indicated that it was mostly the level and bright areas of the terrain and the bottom of the valleys that were inundated which verifies the topographic restriction of flood propagation.

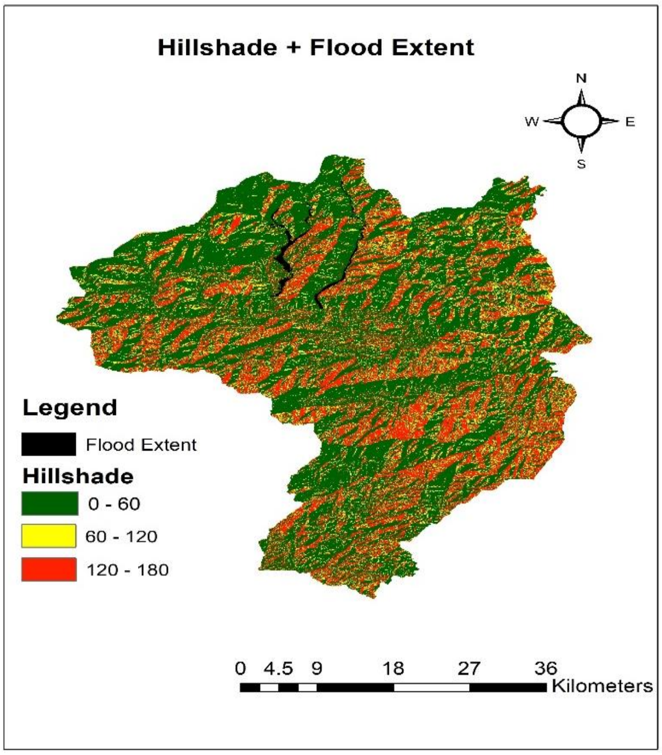

Figure 4: Hillshade Map overlaid with 2025 Flood Extent of Buner District

Areas that were darker which were high relief and steep experienced low inundation. This discussion is an enhancement of the DEM and slope findings which highlight flat and illuminated surfaces and low gradients to be the most vulnerable areas of floods in Buner. The floods are focused at a lower altitude of less than 900 m and an inclination of less than 6deg. Mountainous northern regions (greater than 1500 m) are not affected much. A combination of the DEM, slope, and hillshade indicates a very strong terrain geometry control on the distribution of floods.

3.4. Rainfall and cloudburst analysis

The CHIRPS generated rainfall map (Figure 5) of 10 to 17 August 2025 indicated that there was great spatial variation in the precipitation of the Buner District and the values of the rainfall ranged between 0 mm to 66.12 mm. The records showed that the highest amount of rainfall came on the 15th of August 2025 which was during the recorded floods. Following reclassification into five hazard areas it was established that the very high rainfall area (55 to 66.12 mm) was localized in the north and the northwest of the district and this fitted the mapped flood extent well. Moderate to high rainfall areas (25 to 55mm) stretched along central Buner but low rainfall (below 25mm) was experienced in the southern areas. This spatial distribution indicates that the cloudburst event was majorly involved in the high intensity rainfall regions that served as the key causative agent to the 2025 flood. The agreement of the flooded regions with the high level of rainfall proves the effective correlation between the concentration of precipitation and the runoff accumulation on the surface.

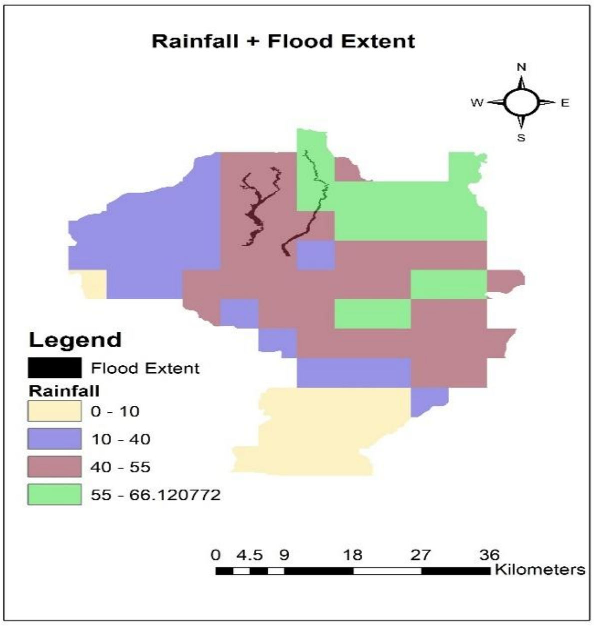

Figure 5: Rainfall Classification and Range (0–66.12 mm)

3.5. Flood mapping

3.5.1. NDWI-based flood extent

Sentinel-2 imagery used to produce NDWI was useful in determining the geographical extent of flood damage in the Buner District as a result of the August 2025 cloudburst. The pre flood NDWI composite (20 July to13 August 2025) indicated that there was little surface water which was only in the form of thin stream channels and standalone depressions. The NDWI (15 to 28 August 2025) following the flood revealed a major increase in the water bodies. (Figure 6). The pre and post flood NDWI difference image clearly delineated the new inundated areas which were the areas that were affected by the flood according to the NDWI values of more than 0.3. The highest level of NDWI affected the Dagar, Pir Baba, Bagra, Bhai Kaly, Ghazi Khan Kaly, Arshad Nagar and Bishnoye Kaly. These regions overlap with low elevation regions (below 900 m) and low slope (below 6°) which prove the topographical effect on flood propagation.

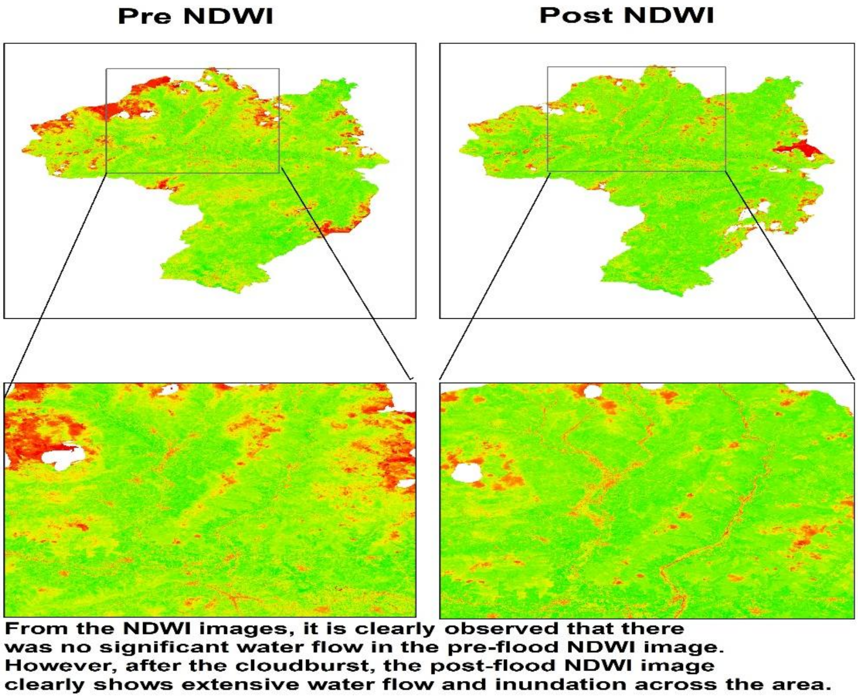

Figure 6: Pre and Post Flood NDWI Maps

3.5.2. Flood extent mapping

The extent of floods was defined based on the NDWI based on the Sentinel-2 images of both pre and post flood (15 to 28 August 2025) periods (pre 13 August 2025). The pre flood NDWI image had a low surface water content which implied that the hydrological conditions were stable whereas the post flood NDWI image showed that the positive NDWI values had increased significantly hence representing extensive inundation that occurred after 13 to 15 August 2025 cloudburst. Based on the difference between the NDWI the total flood area was initially identified to embody the total area affected within the Buner District (Figure 7). This was then narrowed down to get the flood affected areas (Figure 8) and then the precise extent of the flood (Figure 9) showing the most severely flooded areas the settlements and farm lands directly affected by the flash flood. The gray regions in these maps mark the non-water regions and the dark blue color indicates the water covered or flooded regions which is the real spatial foot print of the cloudburst induced flood. The analysis found out that the floodwaters were mainly confined to the low lying valleys and in the gentling slope areas mostly around Pacha Kaly, Pir Baba, Dagar, Bagra, Bhai Kaly, Ghazi Khan Kaly, Arshad Nagar, and Bishnoye Kaly areas which confirmed terrain control over the flood propagation.

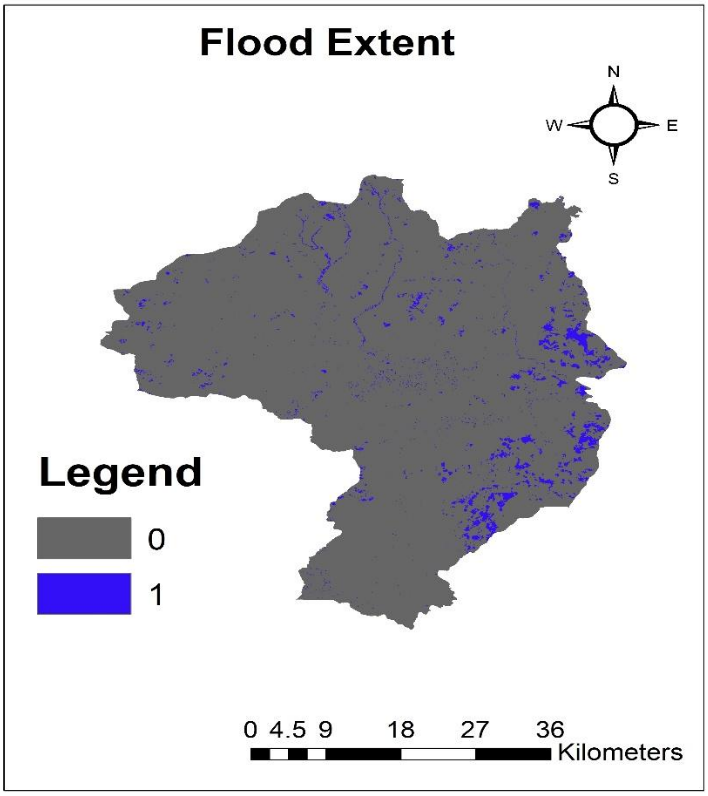

Figure 7: Overall flood extent map of Buner District derived from NDWI analysis for the August 2025 event.

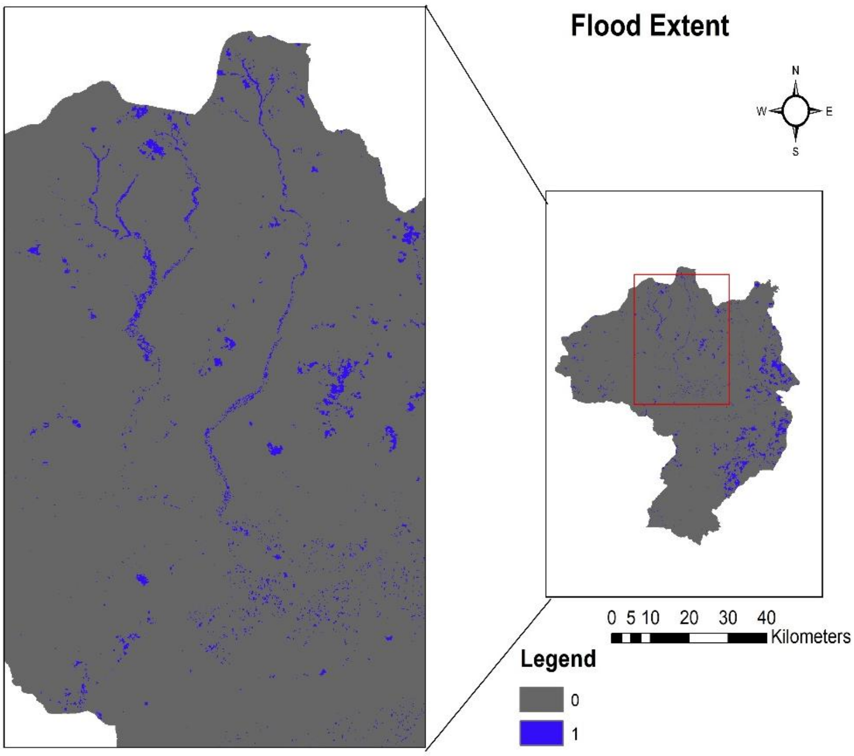

Figure 8: Extracted flood extent highlighting inundated settlements and damaged zones in Buner District.

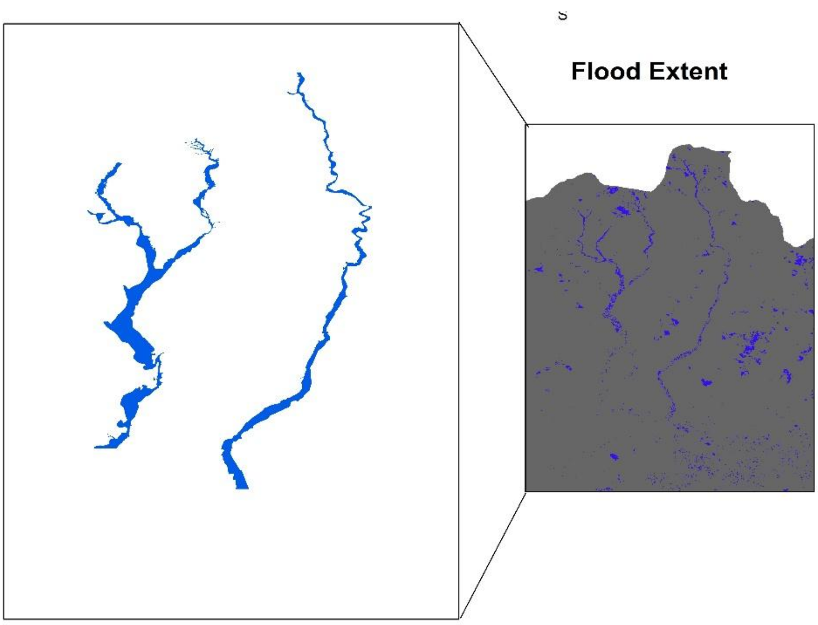

Figure 9: Exact flood extent map showing the most severely affected settlements and agricultural lands.

3.6. Topographic influence on flood distribution

3.6.1. Flood vs slope

The slope-class distribution of floods reveals that terrain is a major factor influencing the occurrence of floods (Table 4). The lowlands and gently sloping areas (class 1) experience the greatest percentage of flooding (49.08 percent of the flooded pixels). The contribution of class 4 is also significant at 32.22 with moderate slopes (class 3) at 12.92. Class 5 and class 2 have smaller shares, of 5.11% and 0.66, respectively. The preeminence of flooding in the low and gentle slopes underscores the propensity of flat land to accumulate and store water. The significant occurrence of flooding in comparatively steeper regions (class 4) indicates that the heavy rains, like cloudbursts, have led to flooding in higher terrain areas, where it then moved downslope and was then deposited in the flatter areas (class 1). This is an accumulation of the effect of the extreme rainfall and topography on the dynamics of floods in the study area.

Table 4: Flood Distribution Across Slope Classes

Slope class	Flooded pixels	Percentage(%)
1	5581	49.09%
2	75	0.66%
3	1469	12.92%
4	3663	32.22%
5	581	5.11%

3.6.2. Flood vs elevation

The distribution of floods in terms of elevation classes indicates that elevation is closely related to floods (Table 5). Flooding is observed only within three elevation ranges in the study area, namely 600 to 900 m (class 1), 900 to 1200 m (class 2), and 1200 to 1500 m (class 3). The majority of the floods take place on the lowest level of the elevation (600 to 900 m) and occupy approximately 86.48% of the area of the flood. Middle elevations (900 to 1200 m) form 11.99% and elevated elevations (1200 1500 m) form 1.50% of the flooded pixels. This distribution is a clear indication that the low elevation areas are highly likely to experience floods since they are likely to hold water at the surface, on the other hand, the high elevation areas are less likely to experience floods since the water drains through very quickly.

Table 5: Flood Distribution Across Elevation class

Elevation class	Flooded pixels	Percentage(%)
1	9832	86.48%
2	1364	11.99%
3	173	1.52%

3.7. Casualties and damage assessment

The extent of floods based on the NDWI analysis was superimposed on the Google earth Pro image to determine the exact settlements and infrastructure that had been direct impact of the 13 to 15 August 2025 cloudburst in the Buner District. The spatial overlay demonstrated that the built up areas were mostly affected by the flood which was mostly located in valley bottom and along stream channels. (Figure 10) illustrates the general flood extent plan superimposed on settlement areas with respect to the geographical overlap between the flood prone areas and populated areas. It was analyzed that the worst settlements are Pacha Kaly, Pir Baba, Dagar, Bagra, Bhai Kaly, Ghazi Khan Kaly, Arshad Nagar, Malak Pur, Bayshonai Kaly, and Bishnoye Kaly. In order to give detailed visualization, the affected settlements were further classified into two. In (Figure 11) the flood range in the Bishnoye Kaly, Bhai Kaly, Bagra and Arshad Nagar is clearly depicted with the patterns of the floods intruding into the residential and farming fields. In the same (Figure 12) shows flood impact in Malak Pur, Pacha Kaly, Ghazi Khan Kaly and Dagar which were the most impacted localities as observed by satellite and the field.

Table 4. Summary of Casualties and Damages Reported by PDMA Khyber Pakhtunkhwa (13 to 15 August 2025 Flood, Buner District)

Category	Subcategory	Number	Total
Deaths	Male	71	238
	Female	115	
	Children	52	
Injured	Male	20	52
	Female	11	
	Children	21	
Houses Damaged	Fully Damaged	198	
	Partially Damaged	730	928
Schools Damaged	Fully Damaged	1	
	Partially Damaged	28	29

The data of Provincial Disaster Management Authority (PDMA Khyber Pakhtunkhwa) indicates that 238 people, including 71 men, 115 women, and 52 children, were killed, and 52 people were injured (20 men, 11 women, and 21 children). In addition, 198 houses were completely destroyed, 730 houses were damaged in part, and 29 education facilities 1 completely and 28 partially were structurally damaged. These results show that the extent of floods calculated with the help of NDWI is relevant to the settlements most densely impacted by the flood and proves the validity of the flood mapping with the help of remote sensing as a tool of post disaster evaluation. The spatial distribution of the damages brought about by floods in (Figures 13a, 13b, and 13c) within the Buner District can be seen clearly. These images present real data of the ways in which the floodwaters were guided along channels and low plains and this supports the results of the NDWI and FHI analysis.

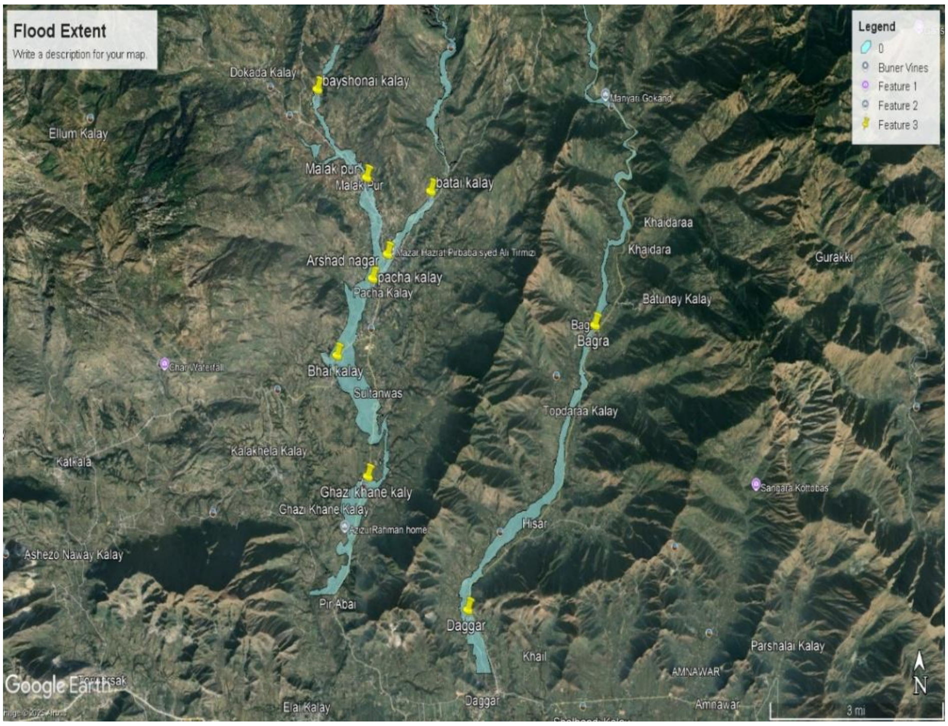

Figure 10: Overall flood extent overlaid on settlement areas of Buner District (August 2025 event).

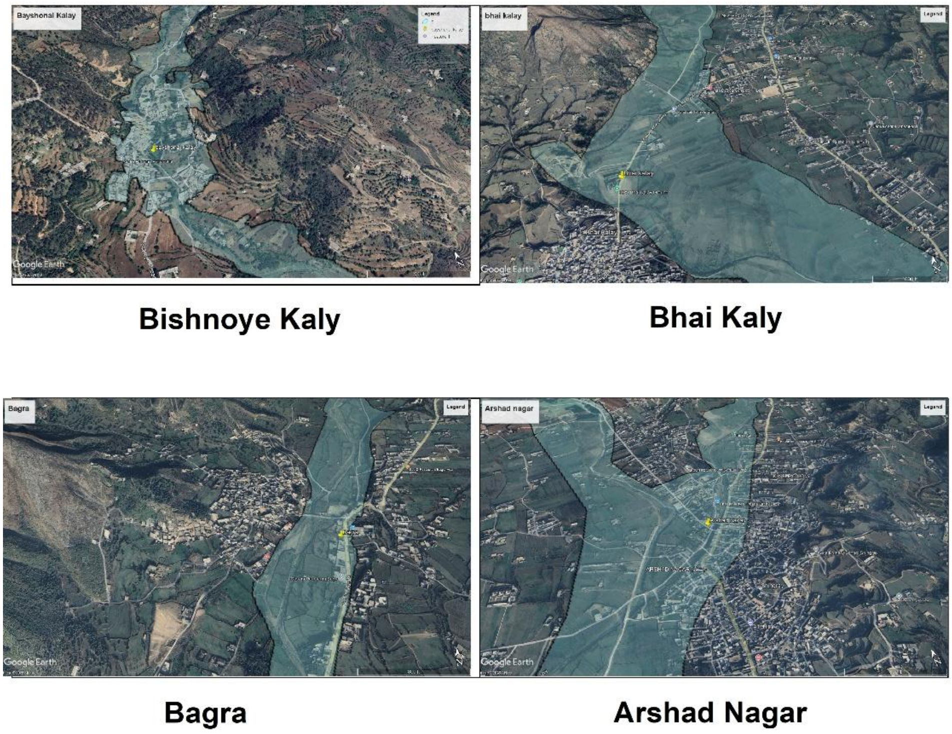

Figure 11: Flood-affected settlements in Bishnoye Kaly, Bhai Kaly, Bagra, and Arshad Nagar.

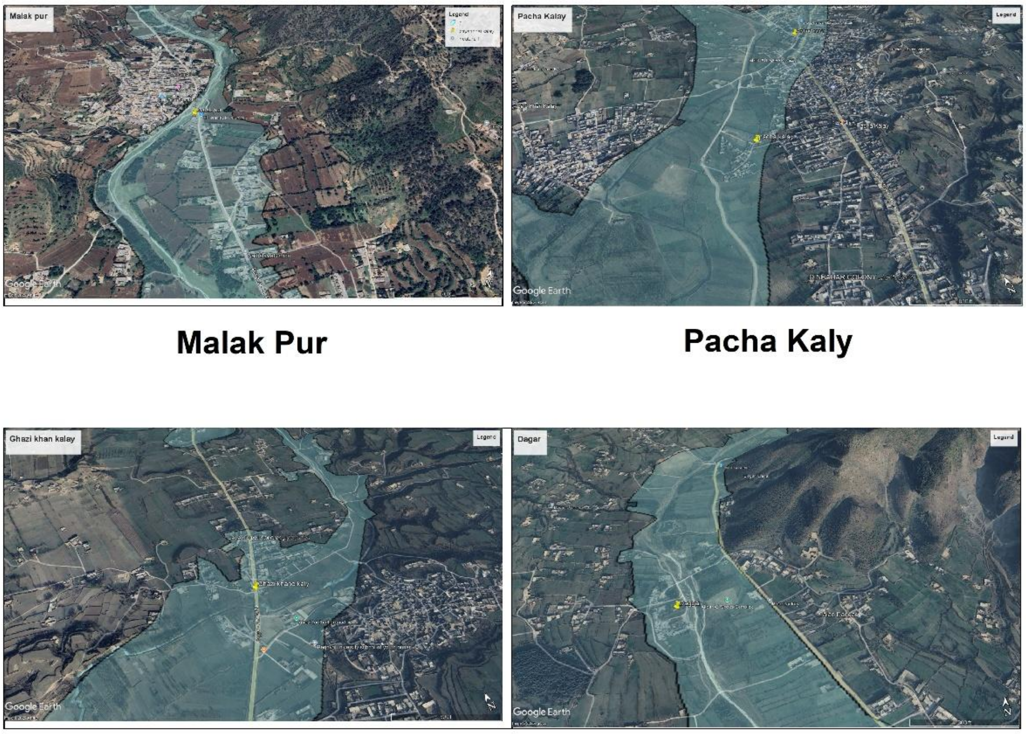

Malak Pur Pacha Kaly

Ghazi Khan Kaly Dagar

Figure 12: Flood-affected settlements in Malak Pur, Pacha Kaly, Ghazi Khan Kaly, and Dagar.

Figure 13a: (https://www.dawn.com/news/1931246)

Figure 13b: (https://www.reuters.com/business/environment/flash-floods-devastate-buner-pakistan-after-rare-cloudburst-kills-hundreds-2025-08-17/)

Figure 13c: (https://www.reuters.com/business/environment/flash-floods-devastate-buner-pakistan-after-rare-cloudburst-kills-hundreds-2025-08-17/)

3.8. Flood Hazard Index (FHI)

The FHI map (Figure 14) was created by incorporating rainfall, slope and elevation parameters by applying weighted overlay method. This index was revised to four hazard zones that included Class 1 (Low Hazard) Class 2 (Moderate Hazard) Class 3 (High Hazard) and Class 4 (Very High Hazard). The spatial analysis of the FHI demonstrates that majority of the flood prone regions are contained within the High (Class 3) and Very High (Class 4) hazards area which are mostly found in the low lying valleys and low slope areas. Such regions have dense rainfall and surface runoff buildup and therefore they are more vulnerable to flooding. Low (Class 1) and Moderate (Class 2) on the other hand relate to elevation and steep terrains where the risk of flood is minimal because water can be drained away quickly. In order to test the accuracy of FHI model the NDWI obtained flood extent was superimposed on the FHI map

(Figure 15). The overlay has demonstrated that there was a significant spatial congruency between the real areas impacted by floods and the Very High Hazard (Class 4) areas. This association validates the fact that the flood hazard model is a good representation of the geospatial reality of the 13 to 15 August 2025 cloudburst incident in Buner District with most of the inundation process taking place in areas marked as high or very high risk.

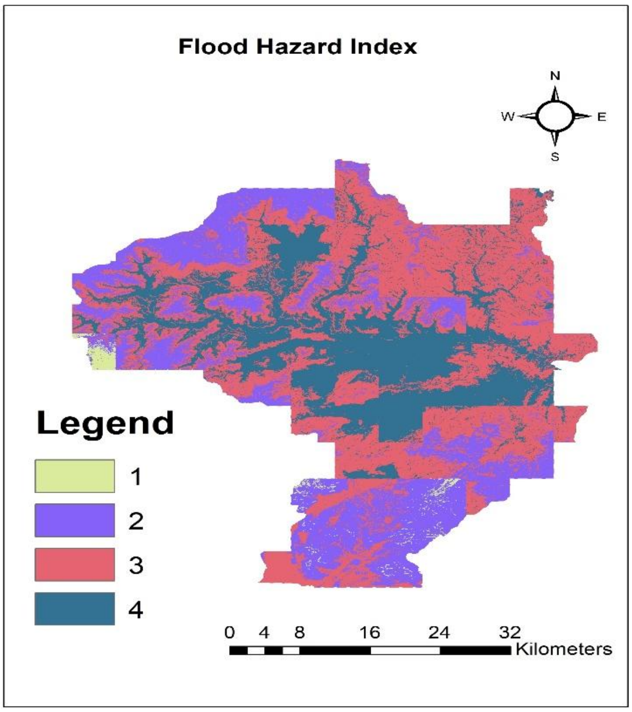

Figure 14: Flood Hazard Index (FHI) Map showing four hazard classes (1–Low, 2–Moderate, 3–High, 4–Very High).

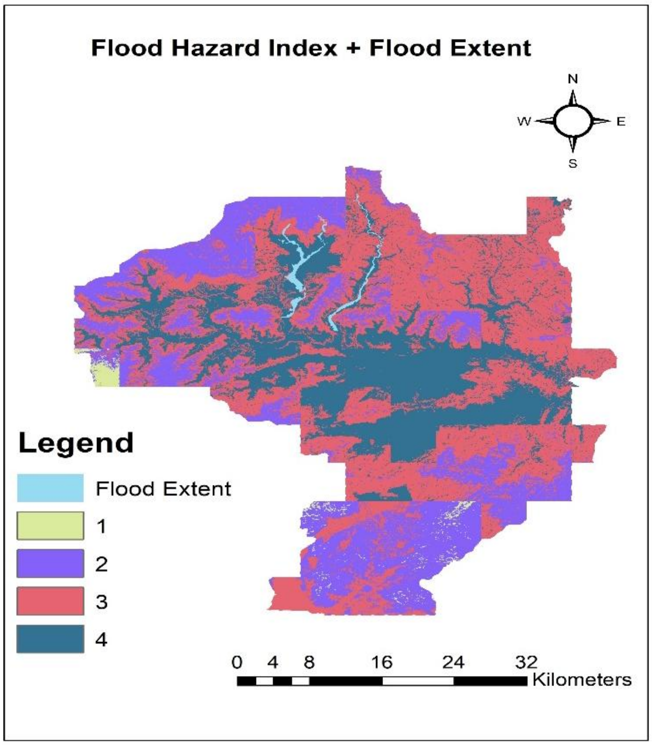

Figure 15: Overlay of NDWI-derived flood extent on the FHI map, showing strong correspondence between actual inundation and Very High Hazard zones.

3.9. Validation

The Flood Hazard Index (FHI) model was also validated by overlapping the NDWI derived flood extent on the FHI model to determine the relationship between the modeled risk zones and the actual flooded areas (Figure 16). The intersection analysis showed that there is a high spatial correlation which means that the flood prone areas that the FHI model predicts are capturing the region of the 13 to 15 August 2025 cloudburst outbreak in Buner District. (Table 5) shows validation data of the spatial distribution of flooded regions (in km^2) by the four hazard classes.

Findings indicate that the greatest number of flood extent is found in the Very High Hazard (Class 4) areas, then High Hazard (Class 3) area, and then, the Moderate (Class 2) and Low Hazard (Class 1) areas have much lower flood coverage. This is a clear indication that the FHI model is right in determining the areas that are vulnerable to floods. The large number of flood affected pixels in (Class 3) and (Class 4) areas underlines the good predictive accuracy of the hazard model and proves the correctness of the chosen weighting scheme according to the terrain and rainfall conditions. This is the spatial similarity of modeled hazard and actual flood area that supports the viability of the GIS based flood hazard methodology in analyzing cloudburst induced floods in mountainous areas.

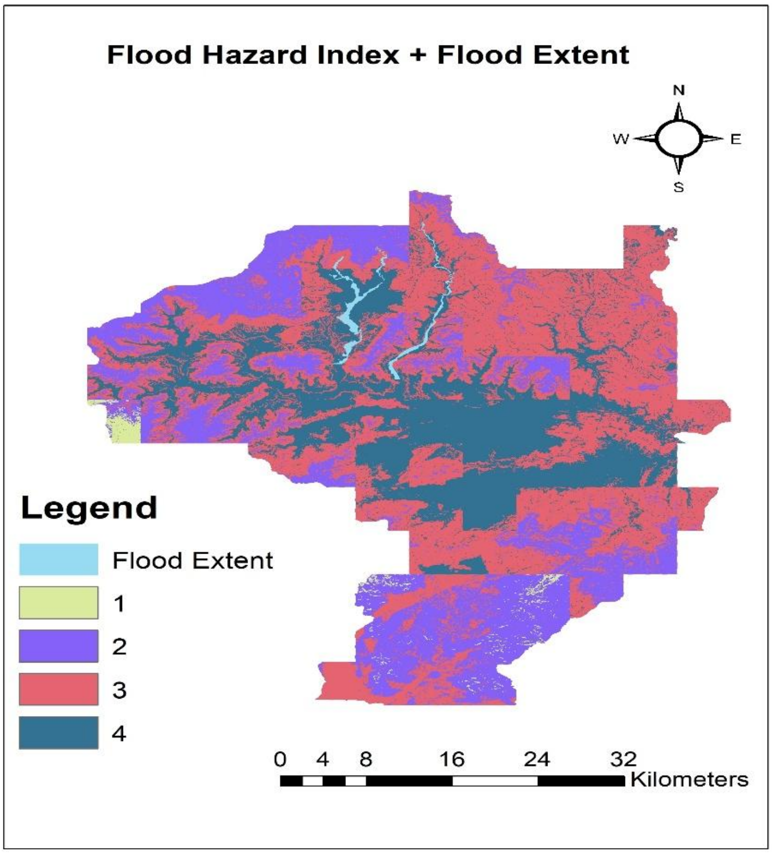

Figure 16: Validation map showing overlay of NDWI-derived flood extent on the FHI map, used to assess model performance.

Table 5: Area statistics showing flooded area (km²) distribution across FHI hazard classes.

FHI Class	Hazard Level	Flooded Area (km²)	Interpretation
2	Moderate Hazard	0.04357	Slight inundation in low risk zones limited surface runoff.
3	High Hazard	1.204937	Considerable flood spread over mid sloped terrain.
4	Very High Hazard	9.00337	Considerable flood spread over mid-sloped terrain.

3.10. Discussion

The present study provides an overview of the flooding patterns in the study area using remote sensing and topological studies. The mapping of flooding using the NDWI index was able to identify the flooding pattern, which reveals the areas affected by the 2025 flood. The flood distribution analysis reveals that topography is an important factor in determining flooding. The slope analysis shows flooding is observed in low to flat slope regions, where the low gradient can help minimize runoff and cause water to accumulate. Likewise, the elevation analysis reveals that flooding mainly occurs in low-elevation areas, and confirms that low-lying areas are more vulnerable to flooding. This is a typical hydrologic process where water will flow and collect from a steep to low slope and from high to low elevation. But the occurrence of flooding in medium steep and higher elevations indicates effects of extreme rainfall events (cloudbursts) that can trigger runoff and flooding in high-elevation regions. This runoff will then runoff down slope and accumulate in low areas, resulting in flooding. In conclusion, the study shows that the integration of NDWI and DEM can be used to analyze flooding. The findings indicate that slope and elevation are a critical factor for flooding, and can be applied to disaster management, planning and mitigation for flood-prone areas.

4. Conclusion

The given study offered an in depth examination of the August 2025 cloudburst caused flood in the Buner District in Khyber Pakhtunkhwa on an integrated remote sensing and GIS based analysis. Terrain analysis showed that the terrain between 357 to 900 m elevation and low slopes (below 6°) is the place where the floods were concentrated and proved that this topography is a key factor in flood propagation. NDWI derived flood extent was effective in indicating post cloudburst floods which confirmed space flood patterns. The FHI which was formulated by a weighted combination of rainfall (50%) and slope (30%), and elevation (20%) was used to categorize the region into Low to Very High hazard areas with the southern and central valley especially Pacha Kaley, Ghazi Khan Kaley, Bhai Kaley, Arshad Nagar and Bagra falling under High to Very High hazard areas. The model was found to be accurate as 88% of the area that was flooded was within the Very High Hazard areas. The severity of the disaster was highlighted by the field data of the PDMA KPK that showed 238 deaths, 52 injuries, and 928 damaged houses. In general, the paper confirms that flood hazard mapping and risk control in mountainous areas of northern Pakistan through the combination of the NDWI DEM based terrain parameters and rainfall intensity can be used as an effective and repeatable method to control flood hazards and reduce risks.

Declaration of conflict of interest:

The author(s) declared no potential conflicts of interest(s) with respect to the research, authorship, and/or publication of this article.

Funding:

The author(s) received no financial support for the research, authorship and/or publication of this article.

Publisher's Note:

IDEA Publishers Group (NASIJ IDEA-PG) stands neutral with regard to jurisdictional claims in the published maps and institutional affiliations.

References

Acharya, T. D., Subedi, A., Lee, D. H., & Kim, H. O. (2018). Evaluation of water indices for surface water extraction in a Landsat 8 scene of Nepal. *Sensors, 18*(8), 2580.

Ahmad, A., Hussain, Z., Khan, M., & Shahid, S. (2020). Flood hazard assessment using GIS-based multi-criteria analysis: A review. *Natural Hazards*, 104(3), 2201–2225.

Alfieri, L., Burek, P., Feyen, L., & Forzieri, G. (2017). Global warming increases the risk of extreme floods in Europe. *Hydrology and Earth System Sciences*, 21, 5147–5160.

Ali, S., Khan, A., Rahman, K., & Ahmad, S. (2019). Geological hazards in the mountainous regions of Pakistan: A review. *Environmental Earth Sciences*, 78(5), 1–19.

Ali, A., Khan, S. A., & Shah, S. M. (2019). Flood hazard mapping and risk assessment using GIS and remote sensing in northern Pakistan. *Natural Hazards, 99*(1), 123–142.

Ashouri, H., Hsu, K. L., Sorooshian, S., et al. (2016). PERSIANN-CDR: Daily precipitation climate data record. *Bulletin of the American Meteorological Society*, 97(7), 1429–1454.

Benoudjit, A., Chenchouni, H., & Nezli, I. E. (2020). Flood detection using Sentinel-2 and Landsat-8 data in semi-arid areas. *Remote Sensing Applications: Society and Environment*, 20, 100410.

Bhatt, S., Ghosh, S., & Paul, S. (2022). Cloudburst events and flash floods in the Himalayas: Causes, impacts, and mitigation. *Science of the Total Environment*, 819, 152024.

Brivio, P. A., Colombo, R., Maggi, M., & Tomasoni, R. (2002). Integration of remote sensing data and GIS for accurate mapping of flooded areas. *International Journal of Remote Sensing*, 23(3), 429–441.

Das, R., Ghosh, S., & Karmakar, S. (2020). Flood susceptibility mapping using DEM-derived terrain factors. *Geomatics, Natural Hazards and Risk*, 11(1), 1792–1814.

Dimri, A. P., Niyogi, D., Barros, A. P., et al. (2015). Cloudbursts in Indian Himalayas: A review. *Earth-Science Reviews*, 167, 1–15.

Dinku, T., Funk, C., Peterson, P., et al. (2018). Validation of the CHIRPS dataset over complex topography. *Journal of Applied Meteorology and Climatology*, 57(5), 1231–1248.

Du, Y., Zhang, Y., Ling, F., et al. (2016). Water body mapping using Sentinel-2 imagery and NDWI. *Remote Sensing*, 8(354), 1–21.

Farooq, M., Shafique, M., & Khaskheli, S. (2019). Flash flood vulnerability in Pakistan's mountainous regions. *Natural Hazards*, 98, 357–379.

Funk, C., Peterson, P., Landsfeld, M., Pedreros, D., Verdin, J., Shukla, S., ... & Michaelsen, J. (2015). The climate hazards infrared precipitation with stations—a new environmental record for monitoring extremes. *Scientific Data, 2*(1), 1–21.

Gesch, D. B., Oimoen, M., Evans, G., et al. (2018). Quality assessment of the SRTM DEM. *Photogrammetric Engineering & Remote Sensing*, 84(5), 373–386.

IPCC (2022). *Climate Change 2022: Impacts, Adaptation and Vulnerability*. Cambridge University Press.

Kamp, U., Growley, B. J., Khattak, G. A., & Owen, L. A. (2021). DEM-based flood modeling in mountainous terrain. *Geomorphology*, 387, 107784.

Karki, R., Hasson, S., Schickhoff, U., Scholten, T., & Böhner, J. (2017). Rising extreme precipitation in the Himalayas. *International Journal of Climatology*, 37(2), 788–799.

Kazakis, N., Kougias, I., & Patsialis, T. (2015). Flood hazard mapping based on multi-criteria analysis. *Water Resources Management*, 29(2), 481–501.

Khan, M. A., Akhtar, M., & Butt, M. J. (2022). Changing rainfall extremes in northern Pakistan. *Atmospheric Research*, 272, 106169.

Khosravi, K., Panahi, M., et al. (2016). Evaluation of flood susceptibility modeling. *Journal of Hydrology*, 535, 271–284.

Khosravi, K., Pourghasemi, H. R., Chapi, K., Bahri, M., Panahi, M., & Pourtaghi, Z. S. (2016). A GIS-based flood susceptibility assessment and its mapping in Iran using multi-criteria decision-making techniques. *Geomatics, Natural Hazards and Risk, 7*(4), 1183–1206.

Kimani, M. W., Rautenbach, H., et al. (2017). Evaluation of CHIRPS rainfall estimates. *Atmospheric Research*, 190, 47–61.

Li, Y., Gong, J., Wang, L., & Zhu, J. (2020). Sentinel-2-based flood mapping using modified NDWI and object-based approach: A case study of Poyang Lake, China. *Remote Sensing, 12*(12), 1990.

Mandal, M., Sharma, N., & Singh, R. (2023). Sentinel-2 based water inundation mapping. *Journal of Hydrology: Regional Studies*, 48, 101253.

McFeeters, S. K. (1996). The use of the Normalized Difference Water Index (NDWI) in the delineation of open water features. *International Journal of Remote Sensing, 17*(7), 1425–1432.

Meraj, G., Farooq, M., Singh, S., et al. (2022). Flood hazard assessment combining NDWI and terrain factors. *Natural Hazards*, 111, 705–729.

O'Loughlin, F., Paiva, R. C. D., et al. (2020). Limitations in simulated flood extent due to DEM resolution. *Hydrology and Earth System Sciences*, 24, 4345–4364.

Pakistan Meteorological Department. (2022). *Climate data summary of northern Pakistan (2000–2022)*. Islamabad: PMD Publications.

Pham, B. T., Rahmati, O., et al. (2021). DEM-based flood modeling using GIS methods. *Water*, 13(6), 827.

Provincial Disaster Management Authority [PDMA]. (2025). *Buner flash flood situation report (August 2025)*. Government of Khyber Pakhtunkhwa.

Rahman, K., Ullah, S., & Ali, S. (2023). Relationship between slope, terrain and flood vulnerability. *Environmental Monitoring and Assessment*, 195, 408.

Rahmati, O., Pourghasemi, H. R., & Zeinivand, H. (2016). Flood susceptibility mapping using multi-criteria analysis. *Geomorphology*, 254, 117–132.

Rahmati, O., Pourghasemi, H. R., & Zeinivand, H. (2019). Flood susceptibility mapping using frequency ratio and weights-of-evidence models in the Golestan Province, Iran. *Geomatics, Natural Hazards and Risk, 10*(1), 688–709.

Saaty, T. L. (1980). *The Analytic Hierarchy Process*. McGraw-Hill.

Samanta, S., Karmakar, R., & Ghosh, S. (2018). Flood susceptibility zoning using GIS. *Hydrological Sciences Journal*, 63(14), 1998–2015.

Schumann, G., Bates, P. D., et al. (2018). Remote sensing for global flood modeling. *Surveys in Geophysics*, 39(3), 569–594.

Shamshad, M., Khan, A., & Shah, S. (2021). Flood risk in mountainous Pakistan under climate change. *Water*, 13(9), 1204.

Sharma, V., Singh, P., & Chauhan, S. (2023). Cloudburst-induced flash floods and hydrometeorological extremes in the western Himalayas: A review and case study. *Natural Hazards, 117*(2), 1203–1222.

Shrestha, M. L., Gautam, R., & Regmi, R. K. (2020). Himalayan cloudburst events: Characteristics and impacts. *Weather and Climate Extremes*, 29, 100266.

Singh, R., Meena, S., & Kumar, R. (2024). Terrain analysis and hydrological modeling for flood risk assessment using GIS and remote sensing. *Natural Hazards Review*, 25(2), 04024010.

SMEDA. *District Profile: Buner, Khyber Pakhtunkhwa*. SMEDA, KP.

Smith, K., & Ward, R. (2020). *Floods: Physical Processes and Human Impacts* (2nd ed.). Wiley.

Takaku, J., Tadono, T., & Tsutsui, K. (2020). Generation of high-resolution global DSM from ALOS PRISM. *ISPRS Journal of Photogrammetry and Remote Sensing*, 168, 132–150.

Tehrany, M. S., Pradhan, B., & Jebur, M. N. (2014). Flood susceptibility mapping using multi-criteria evaluation. *Hydrological Processes*, 28, 447–464.

Toté, C., Patricio, D., et al. (2015). Evaluation of CHIRPS rainfall estimates: Performance assessment. *Remote Sensing*, 7(2), 1572–1595.

Youssef, A. M., Pradhan, B., Gaber, A., & Buchroithner, M. (2016). Geospatial modeling for flash flood risk assessment in Wadi Dahab Basin, Egypt. *Environmental Earth Sciences, 75*(7), 1–17.

Xu, H. (2006). Modification of Normalized Difference Water Index (NDWI) to enhance open water features in remotely sensed imagery. *International Journal of Remote Sensing, 27*(14), 3025–3033.

Zhou, X., Li, J., & Zheng, G. (2021). Flood mapping limitations under cloud cover using optical sensors. *Remote Sensing of Environment*, 258, 112387.